J Math Chem (2014) 52:407–429
DOI 10.1007/s10910-013-0269-x

ORIGINAL PAPER

Local topology at limited resource induced suboptimal traps on the quantum control landscape

Ashley Donovan · Vincent Beltrani · Herschel Rabitz

Received: 6 August 2013 / Accepted: 3 October 2013 / Published online: 18 October 2013

Abstract In a quantum optimal control experiment a system is driven towards a target observable value with a tailored external field. The underlying quantum control landscape, defined by the observable as a function of the control variables, lacks suboptimal extrema upon satisfaction of certain physical assumptions. This favorable topology implies that upon climbing the landscape to seek an optimal control field, a steepest ascent algorithm should not halt prematurely at suboptimal critical points, or traps. One of the important aforementioned assumptions is that no limitations are imposed on the control resources. Constraints on the control restricts access to certain regions of the landscape, potentially preventing optimal performance through convergence to limited resource induced suboptimal traps. This work develops mathematical tools to explore the local landscape structure around suboptimal critical points. The landscape structure may be favorably altered by systematically relaxing the control resources. In this fashion, isolated suboptimal critical points may be transformed into extensive level sets and then to saddle points permitting further landscape ascent. Time-independent kinematic controls are employed as stand-ins for traditional dynamic controls to allow for performing a simpler constrained resource landscape analysis. The kinematic controls can be directly transferred to their dynamic counterparts at any juncture of the kinematic analysis. The numerical simulations employ a family of landscape exploration algorithms while imposing constraints on the kinematic controls. Particular algorithms are introduced to meet the goals of either climbing the landscape or seeking specific changes in the topology of the landscape by relaxing the control resources.

Keywords Quantum control · Quantum theory · Constrained quantum control · Constrained quantum control landscapes

---

A. Donovan · V. Beltrani · H. Rabitz (✉)
Department of Chemistry, Princeton University, Princeton, NJ, USA
e-mail: hrabitz@princeton.edu

1 Introduction

A quantum control experiment typically aims to identify a tailored radiation pulse that enables achieving a high fidelity for a target objective value. Continued improvements in laser pulse-shaping and detection techniques as well as computer learning algorithms have led to a growing number of successful experiments ([9,11,13,18]; for an overview, see [2]). In addition to the experimental advances, quantum control theory has rapidly developed along with extensive numerical simulations [1,5,10,19,29,33,32]. The generally good performance of quantum control experiments and simulations has been attributed to the attractive topology of the underlying quantum control landscape, which is the observable as a function of the control variables [20]. Searching for an optimal control thus entails climbing the landscape aiming to reach a global extremum. The present work considers the observable as the state-to-state transition probability $P_{i\to f}$,

$$P_{i\to f} = |\langle f|U(T,0)|i\rangle|^2, \tag{1}$$

where $U(t,0)$ is the unitary time-evolution operator satisfying the time-dependent Schrödinger equation

$$\imath\hbar\frac{\partial}{\partial t}U(t,0) = H(t)U(t,0), \qquad U(0,0) = \mathbb{1}. \tag{2}$$

In Eq. (1), T is the target time and the Hamiltonian $H(t)$ depends on the dynamic control $\varepsilon(t)$. Formally, $U(T,0)$ may be written as

$$U(T,0) = \mathcal{T}\exp\left(-\frac{\imath}{\hbar}\int_0^T H(t)dt\right) \tag{3}$$

with $\mathcal{T}$ being the time-ordering operator. A critical point of the $P_{i\to f}[\varepsilon(t)]$ landscape is defined as

$$\frac{\delta P_{i\to f}}{\delta\varepsilon(t)} = 0, \qquad \forall t \in [0,T]. \tag{4}$$

Landscape critical points are of special interest as they correspond to locations where a climb, to first order [c.f., Eq. (4)], stops. When specific Assumptions are satisfied, the $P_{i\to f}[\varepsilon(t)]$ landscape is free of suboptimal trapping critical points, thus permitting ready ascent of the landscape approaching $P_{i\to f} = 1.0$ [20]. The first Assumption is that the quantum system is controllable [27,23], and the second Assumption is that $\delta U(T,0)/\delta\varepsilon(t)$ is full rank. These two Assumptions appear to be readily satisfied in many cases [16]. The third Assumption, which is most salient to the present work, is that the control resources $\varepsilon(t)$ are free of constraints, which permits unfettered access to all regions of the control landscape. However, experiments are inherently subject to constraints. For example, laser pulses are restricted to lie within a limited bandwidth

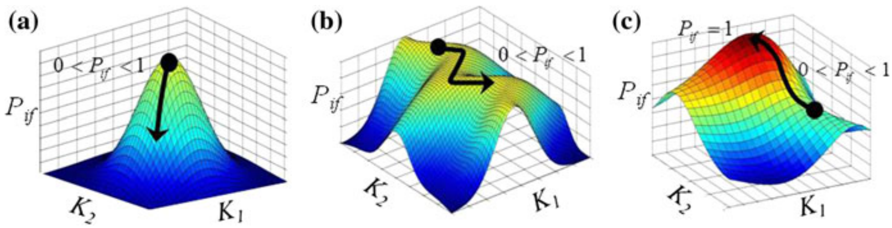

Fig. 1 (Color available online) Distinct possible local landscape topologies at suboptimal transition probability landscape critical points; the same topological behavior would also apply to more general control observables. Two controls, K_1 and K_2, are shown for illustration, but in practice there will be many more control variables. Plot **a** shows a trap existing as an isolated point on the landscape, where any change to the controls results in a decrease in $P_{i\to f}$ along the indicated trajectory. Plot **b** shows a trap residing on a level set, forming a suboptimal submanifold of solutions where suitable changes to the controls along the trajectory can preserve the suboptimal $P_{i\to f}$ value. Plot **c** shows a saddle, where subsequent changes to the controls along an appropriate path permit increasing $P_{i\to f}$, possibly to a higher yield trap or even the maximum $P_{i\to f} = 1.0$

about some operational frequency [24], although bandwidth expansion and frequency shifting techniques are becoming more prevalent [4,8,3]. While mathematically proving that the $P_{i\to f}$ landscape is free of suboptimal critical points calls for unrestricted access to all controls, in practice good if not fully optimal performance is expected with a judicious choice of resources (e.g., operation with phase and amplitude-modulated control fields at or near the system's natural transition frequencies). Little is known about the boundary between adequate resources and where further enchroachment will introduce suboptimal landscape critical points.

Numerous works have incorporated specific constraints in quantum control simulations, including spectral component restrictions [30,12,31] and limitations on phase controls [14,28]. Understanding the role of constraints on the ability to achieve optimal quantum control remains an important goal and motivates the present work. Constraints may be viewed as limiting access to certain regions of the landscape, and as a result possibly introducing suboptimal extrema whose encounter upon optimization could prohibit reaching the maximum yield. Such limited resource induced suboptimal extrema may be viewed as artificial landscape features, as they arise due to restricted access to the underlying trap-free landscape. However, in the laboratory or in simulations these features will appear to be real when employing significant control constraints. This work presents mathematical tools to *explore* and *systematically alter* the local landscape structure around such suboptimal critical points, which include saddles and traps. Figure 1 illustrates three distinct topological scenarios that may be encountered at a constraint-induced trap. Figure 1a shows a trap existing as a point where the local landscape curvature is negative, implying that any variation to the constrained controls K_1, K_2 will result in a reduced observable value, as shown by the decreasing trajectory for $P_{i\to f}$. Figure 1b shows a trap that resides on a manifold of suboptimal solutions (rather than a point), and the path depicted by the arrow shows that careful variation of the constrained controls can permit moving along this submanifold, referred to as a suboptimal observable-preserving level set. Figure 1c indicates a saddle, where suitable variation of the constrained controls can lead to improved or even optimal control, as shown by the increasing trajectory for $P_{i\to f}$.

A dynamic control $\varepsilon(t)$ can include large numbers of variables such as frequency-dependent phases and amplitudes; as such, a general constrained dynamic landscape assessment is difficult to attain, especially as the evolution operator $U(t, 0)$ can depend upon the control in a complex manner. As a means to simplify the control landscape analysis, we will utilize the identity

$$U = \exp(\imath A) \tag{5}$$

where A is a Hermitian matrix that ensures unitarity of $U \equiv U(T, 0)$ [20]. The matrix elements of A have been conveniently treated as time-independent 'kinematic' control variables in previous works [6,15,21]. These control variables subsume the time-dependence of the Hamiltonian, and much has been learned about control landscape topology using kinematic variables. The present work will utilize these simpler kinematic controls to investigate constrained landscape topology.

The unconstrained landscapes $P_{i\to f}[A]$ and $P_{i\to f}[\varepsilon(t)]$ share the same topology [20]. This work aims to explore the topological features of the constrained $P_{i\to f}[A]$ landscape resting on the foundation that kinematic controls can be directly transferred to their dynamic control counterparts by equating Eqs. (3) and (5),

$$\mathcal{T}\exp\left(-\frac{\imath}{\hbar}\int_0^T H(t)dt\right) = \exp(\imath A). \tag{6}$$

Assuming that the system is controllable [23,27], then Eq. (6) may be used to formulate a practical methodology for converting from kinematic to dynamic controls, $A \to \varepsilon(t)$, and generally $\varepsilon(t)$ will not be unique for a specified A. The transformation $A \to \varepsilon(t)$ can be implemented in a variety of ways, depending on whether each element of U in Eq. (6) is to be preserved or at the other extreme where only the $P_{i\to f}$ value (i.e., the norm of a single element of U) is asked to be maintained when identifying $\varepsilon(t)$. The present work focuses on exploiting kinematic controls, with consideration of the kinematic $\to$ dynamic mapping left for a future study [7]. However, the capability of performing such a transferral [17] provides a supporting foundation for the work here.

The paper is structured as follows. Section 2 presents the mathematical tools to explore the local landscape around a limited resource induced suboptimal critical point. Gradient-based optimization is utilized to guide constrained controls towards the closest, steepest ascent-accessible critical point. The neighborhood of an isolated critical point can be explored as a basis to guide systematic relaxation of the control constraint in order to seek the formation of a suboptimal observable-preserving level set of controls. The latter freedom to alter critical point character can be important, as particular locations on suboptimal level sets may have distinct features (e.g., desirable robustness to control perturbations). Further enhancement of the control resources may also convert a suboptimal trapped level set into a saddle permitting continued ascent of the landscape. Section 3 presents numerical illustrations that utilize the mathematical techniques from Sect. 2 to examine the variety of landscape topologies at suboptimal critical points illustrating the circumstances in Fig. 1. Section 4 provides concluding remarks.

2 Mathematical formulation

The search over a set of constrained control variables that produce the highest possible observable value occurs on the quantum control landscape. Generally, the presence of constraints will restrict free traversal of the landscape, in some a priori unknown manner. To ameliorate the complexity of performing a dynamic landscape analysis, this work uses time-independent kinematic controls, which are the elements of the N-dimensional Hermitian matrix A in Eq. (5). We consider real symmetric A matrices, which in itself may be viewed as a constraint on the space of admissible controls, though it still permits up to $M = N(N+1)/2$ variables (i.e., complex Hermitian A matrices have up to N^2 variables). Previous work showed that at least $2N-2$ variables are generally required to achieve optimal $P_{i\to f}$ control [15,14,22], thus we still have $M > 2N-2$. However, an inappropriate set of even more than $2N-2$ controls can still present a significant limitation. The control variables can be collected into a length-M vector

$$K = [A_{11}, A_{12}, \ldots, A_{NN}] \tag{7}$$

where K_m denotes the mth control variable.

The remainder of Sect. 2 is organized as follows. Section 2.1 presents the local search procedure used for ascending the $P_{i\to f}[A]$ landscape to achieve the highest possible yield when the controls are subject to a constraint. This algorithm is a constraint-adopted form of the D-MORPH [25,26] procedure. Section 2.2 derives an equation for the constrained Hessian (i.e., the matrix of second-order derivatives of $P_{i\to f}$ with respect to the control variables) at a suboptimal critical point to elucidate local landscape structure. In particular, the nature of the eigenvalue spectrum of the Hessian can differentiate saddles from traps, and further distinguish traps that exist as points (Fig. 1a) from those that exist as part of a set of connected suboptimal controls (Fig. 1b). In the former case, it is possible to systematically relax the originally serious constraint and then explore the range of connected families of controls that form a level set for the trap using a procedure presented in Sect. 2.3. Section 2.4 also considers relaxation of the constrained controls to transform the situation in Fig. 1a into that of Fig. 1c for climbing higher on the landscape. These capabilities address the important practical aim of assessing the possible gains in desirable performance and yield at the expense of enhancing the still limited control resources. Table 1 summarizes the goals and associated key equations developed in Sect. 2.

2.1 Climbing the $P_{i\to f}$ landscape with constrained control resources

The goal of the constrained D-MORPH algorithm used in this work is to systematically vary the controls K [c.f., Eq. (7)] in order to maximize $P_{i\to f}$ while maintaining a control constraint denoted as C. Such a circumstance may arise dynamically in many ways (e.g., the pulse fluence is constant). The procedure introduces an optimization progress parameter s such that $K \to K(s)$ and subsequently $P_{i\to f}[K] \to P_{i\to f}[K(s)]$. To first order, increasing $P_{i\to f}$ requires satisfying

Table 1 Summary of goals, variables, and relevant equations for the landscape critical point exploration techniques developed in Sect. 2

Goal	Reach critical point under an imposed constraint	Move on a trap level set	Vary trap topology by altering the constraint
Subsection	2.1	2.3	2.4
Variables	K	K	c
Morphing parameter	s	r	u
Differential equation	$\frac{dK}{ds} = \mathcal{P}_{\nabla C} \nabla P_{i\to f}$	$\frac{dK}{dr} = \mathcal{P}_{\nabla C} \mathcal{P}_{\tilde{\mathcal{H}}} g'$	$\frac{dc}{du} = \mathcal{P}_{\Omega} h$
Comments	Trap conditions: $dP_{i\to f}/ds = 0$; $\nabla P_{i\to f}$ and ∇C are parallel	g' chosen to satisfy an ancillary cost function	Create a level set by choosing h to minimize $\mathcal{L}_1$ in Eq. (42) Create a saddle by choosing h to maximize $\mathcal{L}_2$ in Eq. (45)

See the indicated Subsection for details

$$\frac{dP_{i\to f}}{ds} = \nabla P_{i\to f}^{\top} \frac{dK}{ds} \geq 0, \tag{8}$$

where $\nabla P_{i\to f}$ is a length-M column vector containing elements $\partial P_{i\to f}/\partial K_m, m = 1, \ldots, M$ with [6]

$$\frac{\partial P_{i\to f}}{\partial K_m} = -2\mathrm{Im}\left(\langle i|U^{\dagger}|f\rangle\langle f| \int_0^1 du\, \exp[\imath(1-u)A] \frac{\partial A}{\partial K_m} \exp(\imath u A)|i\rangle \right). \tag{9}$$

Here $\partial A/\partial K_m$ is an $N \times N$ matrix with 1 in the position(s) corresponding to the mth control variable and zeros elsewhere. Let $C(s) := C[K(s), c]$ denote a constraint function that depends on the control variables K as well as a set of L constraint parameters $c = [c_1, \ldots, c_L]$ that are independent of s. The parameters c depend upon the nature of C and will be specified in each particular application. The constraint is imposed by demanding that $C[K(s), c] = C_0$ be maintained for some specified constant value of C_0 as $K(s)$ is varied. The present work assumes a single constraint C for clarity, but the formulation may be generalized to a set of simultaneously imposed constraints. Satisfying $C = C_0$ to first order requires

$$\frac{dC}{ds} = \nabla C^{\top} \frac{dK}{ds} = 0, \tag{10}$$

where ∇C is a length-M vector containing elements $\partial C/\partial K_m, m = 1, \ldots, M$. The goal is to identify a differential equation for $K(s)$ such that Eqs. (8) and (10) are simultaneously satisfied. To this end, we define the $M \times M$ positive semidefinite projector $\mathcal{P}_{\nabla C} = (\mathbb{1} - \nabla C(\nabla C^{\top}\nabla C)^{-1}\nabla C^{\top})$ and let

$$\frac{dK}{ds} = \mathcal{P}_{\nabla C} f(s). \tag{11}$$

Any choice for $f(s)$ will ensure satisfaction of Eq. (10) since $\nabla C^\top \mathcal{P}_{\nabla C} = 0$, and setting $f(s) = \nabla P_{i\to f}$ will concomitantly satisfy Eq. (8). Integrating the M differential equations in Eq. (11) will produce a trajectory $K(s)$ that will evolve over s until $dP_{i\to f}/ds = 0$, to specified precision. The unconstrained landscape analysis showed that critical points where $\nabla P_{i\to f} = 0$, which forces $dP_{i\to f}/ds = 0$ [c.f., Eq. (8)], only occur at $P_{i\to f} = 0$ or 1 [20]. However, due to the imposition of C, it may be possible that $dP_{i\to f}/ds = 0$ when $\nabla P_{i\to f} \neq 0$ and $0 < P_{i\to f} < 1$, i.e., when the controls become stuck at a local trap where $dK/ds = 0$ as $s \to \infty$. Substituting Eq. (11) into Eq. (8) with $f(s) = \nabla P_{i\to f}$ yields the trap criterion $\nabla P_{i\to f}^\top \mathcal{P}_{\nabla C} \nabla P_{i\to f} = 0$, which implies that the gradients $\nabla P_{i\to f}$ and ∇C are parallel at a critical point.

2.2 Elucidating the character of constraint-induced critical points

At a suboptimal critical point where $dP_{i\to f}/ds = 0$, the second derivative of $P_{i\to f}$ (i.e., the Hessian) needs to be investigated to deduce whether a trap or a saddle has been encountered. As background, at the top of the unconstrained $P_{i\to f}$ landscape, the Hessian has at most $2N-2$ negative eigenvalues, where the remaining eigenvalues are zero [22]. The Hessian eigenvectors associated with the negative eigenvalues reveal how the controls may be varied in a coordinated manner to move off the top of the landscape. The zero eigenvalues have associated eigenvectors indicating how the controls may be varied while maintaining $P_{i\to f} = 1.0$ to second order. Importantly, when control variables are subject to constraints, the unconstrained Hessian matrix with elements $\partial^2 P_{i\to f}/\partial K_m \partial K_n$ generally does not provide a proper description of the local curvature at suboptimal critical points. The 'constrained Hessian,' derived below, reveals the true local landscape structure at a constraint-induced critical point.

To distinguish between the present excursions in the neighborhood of a local suboptimal critical point and the initial landscape ascent, a new variable r is introduced such that $K \to K(r)$ and $C \to C[K(r), c]$ (see Table 1). The analysis below considers that a landscape climb has already been performed to reach a constraint-induced critical point at a suboptimal value $P_{i\to f} < 1.0$ that will be maintained to second order while $K(r)$ is varied such that $dP_{i\to f}/dr = 0$ and $d^2 P_{i\to f}/dr^2 = 0$. These criteria give

$$\frac{1}{2}\left(\frac{dK}{dr}\right)^\top \nabla^2 P_{i\to f} \frac{dK}{dr} \Delta r^2 + \frac{1}{2} \nabla P_{i\to f}^\top \frac{d^2 K}{dr^2} \Delta r^2 = 0. \tag{12}$$

Similarly, the constraint $C(r) = C_0$ is demanded to be maintained up to second order, giving

$$\frac{1}{2}\left(\frac{dK}{dr}\right)^\top \nabla^2 C \frac{dK}{dr} \Delta r^2 + \frac{1}{2} \nabla C^\top \frac{d^2 K}{dr^2} \Delta r^2 = 0. \tag{13}$$

Rewriting Eq. (13) as

$$\nabla C^{\top} \frac{d^2 K}{dr^2} = -\left(\frac{dK}{dr}\right)^{\top} \nabla^2 C \frac{dK}{dr} \tag{14}$$

and then multiplying on the left by $\nabla C(\nabla C^{\top} \nabla C)^{-1}$ yields

$$(\mathbb{1} - \mathcal{P}_{\nabla C})\, \frac{d^2 K}{dr^2} = -\nabla C(\nabla C^{\top} \nabla C)^{-1} \left(\frac{dK}{dr}\right)^{\top} \nabla^2 C \frac{dK}{dr}. \tag{15}$$

Multiplying Eq. (15) by $\nabla P_{i\to f}^{\top}$ and noting that $\nabla P_{i\to f}^{\top} \mathcal{P}_{\nabla C} = 0$ at a critical point (see Sect. 2.1) produces

$$\nabla P_{i\to f}^{\top} \frac{d^2 K}{dr^2} = -\nabla P_{i\to f}^{\top} \nabla C(\nabla C^{\top} \nabla C)^{-1} \left(\frac{dK}{dr}\right)^{\top} \nabla^2 C \frac{dK}{dr}. \tag{16}$$

From Eq. (12),

$$\nabla P_{i\to f}^{\top} \frac{d^2 K}{dr^2} = -\left(\frac{dK}{dr}\right)^{\top} \nabla^2 P_{i\to f} \frac{dK}{dr}. \tag{17}$$

Combining Eqs. (16) and (17) and rearranging yields

$$\left(\frac{dK}{dr}\right)^{\top} \left(\nabla^2 P_{i\to f} - \nabla P_{i\to f}^{\top} \nabla C(\nabla C^{\top} \nabla C)^{-1} \nabla^2 C\right) \frac{dK}{dr} = 0. \tag{18}$$

The term $\nabla^2 P_{i\to f}$, with elements $\partial^2 P_{i\to f}/\partial K_m \partial K_n$, is the unconstrained Hessian matrix, while the term $\nabla P_{i\to f}^{\top} \nabla C(\nabla C^{\top} \nabla C)^{-1} \nabla^2 C$ incorporates the imposed constraint. The constrained Hessian matrix $\mathcal{H}$ can then be identified from Eq. (18) as

$$\mathcal{H} = \nabla^2 P_{i\to f} - \nabla P_{i\to f}^{\top} \nabla C(\nabla C^{\top} \nabla C)^{-1} \nabla^2 C, \tag{19}$$

and Eq.(18) becomes

$$\left(\frac{dK}{dr}\right)^{\top} \mathcal{H} \left(\frac{dK}{dr}\right) = 0. \tag{20}$$

This equation may be interpreted as specifying a differential change in the controls, dK/dr, that also leaves the value of $P_{i\to f}$ invariant at a constraint-induced suboptimal critical point. The constrained Hessian can be written in terms of its eigenvalues λ_i and eigenvectors ν_i,

$$\mathcal{H} = \sum_{i=1}^{M} \lambda_i \nu_i \nu_i^{\top}, \tag{21}$$

which can be used to understand the local landscape structure around a suboptimal critical point. Section 2.3 will show how to vary the controls while staying on a critical point level set based on the eigenstructure of the constrained Hessian (i.e., suggested by Fig. 1b, c). Note that if all of the eigenvalues are negative, $\{\lambda_i < 0\}$, then the suboptimal constraint-induced critical point is isolated as in Fig. 1a. Section 2.4 will then show how to systematically change the form of the constrained resources to transition from Fig. 1a to Fig. 1b or c.

2.3 Moving on a suboptimal critical point level set

We seek to explore the local landscape level set around a suboptimal critical point by identifying dK/dr such that Eq. (20) is satisfied. Towards this goal, a change in K that preserves the constraint $C = C_0$ implies that

$$\frac{dK}{dr} = \mathcal{P}_{\nabla C}\, g \tag{22}$$

where the function g will be specified below. Introducing Eq. (22) into Eq. (20), we define the projected Hessian as

$$\tilde{\mathcal{H}} = \mathcal{P}_{\nabla C}\mathcal{H}\mathcal{P}_{\nabla C}, \tag{23}$$

such that

$$g^\top \tilde{\mathcal{H}} g = 0. \tag{24}$$

Equation (24) dictates that g must lie in the nullspace of $\tilde{\mathcal{H}}$, thereby specifying the right-hand side of Eq. (22). The projector $\mathcal{P}_{\nabla C}$ introduces into $\tilde{\mathcal{H}}$ the same number of 'trivial' zero eigenvalues as the number of imposed constraints. In this work, we consider only a single constraint so that the presence of a level set requires that $\tilde{\mathcal{H}}$ have at least two zero eigenvalues. Let $J < M - 1$ denote the number of remaining non-zero $\tilde{\mathcal{H}}$ eigenvalues. The projected Hessian $\tilde{\mathcal{H}}$ can be written analogously to Eq. (21) as a sum

$$\tilde{\mathcal{H}} = \sum_{j=1}^{J} \tilde{\lambda}_j \tilde{\nu}_j \tilde{\nu}_j^\top, \tag{25}$$

where $\tilde{\lambda}_j$ is the non-zero projected Hessian eigenvalue associated with the eigenvector $\tilde{\nu}_j$. Eq. (24) can be rewritten as

$$g^\top \left(\sum_{j=1}^{J} \tilde{\lambda}_j \tilde{\nu}_j \tilde{\nu}_j^\top \right) g = 0, \tag{26}$$

which requires that $\tilde{\nu}_j^\top g = 0$ for all j. The function g can then be defined as

$$g = \left(\mathbb{1} - \sum_{j=1}^{J} \tilde{\nu}_j \tilde{\nu}_j^{\top} \right) g' \tag{27}$$

$$= \mathcal{P}_{\tilde{\mathcal{H}}} g' \tag{28}$$

for some arbitrary function g' that may be chosen to satisfy an ancillary cost as desired and $\mathcal{P}_{\tilde{\mathcal{H}}}$ projects into the nullspace of $\tilde{\mathcal{H}}$. Combining all of the above steps gives

$$\frac{dK}{dr} = \mathcal{P}_{\nabla C} \mathcal{P}_{\tilde{\mathcal{H}}} g', \tag{29}$$

which will ensure that changes in K lie in the nullspace of $\tilde{\mathcal{H}}$ while preserving the critical point criteria.

2.4 Varying the form of the constraint to alter critical point topology

Recall that the constraint C is a function of the controls K as well as the constraint parameters c. In the formulation for climbing the landscape subject to a constraint (Sect. 2.1) and for moving along a suboptimal level set (Sect. 2.3), there was no variation permitted in c, thereby maintaining the *form* of the control constraint. In practice, constraints on the controls may be considered for relaxation if desirable variation of landscape topology can be achieved. The case of particular interest is an initially constrained control form producing a suboptimal trap as an isolated landscape point, where it is not possible to vary K without decreasing $P_{i\to f}$ (see Fig. 1a). Here we present a systematic procedure to relax the constraint parameters c with the goal of converting the isolated trap into either (i) a suboptimal level set (Fig. 1b) or (ii) a saddle permitting a further increase in $P_{i\to f}$ (Fig. 1c). Considering that the goals here are distinct from those in Sects. 2.1–2.3, we define u (see Table 1) as a new parameter where $c \to c(u)$ such that $C(u) := C[K, c(u)]$. In order to emphasize that just the form of the control constraint is being altered, we demand that $C[K, c(u)] = C_0$ be maintained as a constant while $c(u)$ evolves. Additionally, at this stage of altering the form of the constraint, the control K is fixed at its original critical point value; after morphing c, then the control K can again be varied within the new form of the constraint to take advantage of the altered local landscape topology.

As stated above, the first condition imposed during the morphing of $c(u)$ is that $C = C_0$ be maintained, or

$$\frac{dC}{du} = \sum_{l=1}^{L} \frac{\partial C}{\partial c_l} \frac{dc_l}{du} = 0. \tag{30}$$

Thus, dc/du must satisfy

$$\nabla_c C^{\top} \frac{dc}{du} = 0, \tag{31}$$

where $\nabla_c C$ is the length-L vector with elements $\partial C / \partial c_l$.

During the variation of c, the gradients $\nabla P_{i\to f}$ and ∇C need to remain parallel to assure satisfaction of the critical point condition $\mathcal{P}_{\nabla P_{i\to f}}\nabla C = 0$. The $M \times M$ projector $\mathcal{P}_{\nabla P_{i\to f}}$ (defined analogously to $\mathcal{P}_{\nabla C}$ as in Sect. 2.1) has one identically zero eigenvalue, which implies that it can be written in terms of its $R = M - 1$ non-zero eigenvalues σ and corresponding eigenvectors w as

$$\mathcal{P}_{\nabla P_{i\to f}} = \sum_{j=1}^{R} \sigma_j w_j w_j^\top. \tag{32}$$

Maintaining the gradients $\nabla P_{i\to f}$ and ∇C as parallel implies that

$$\mathcal{P}_{\nabla P_{i\to f}}\nabla C = \sum_{j=1}^{R} \sigma_j w_j w_j^\top \nabla C = 0, \tag{33}$$

which requires

$$w_j^\top \nabla C = 0 \tag{34}$$

for all j and u. With the goal of obtaining an equation for $c(u)$, we may differentiate Eq. (34) to form

$$\frac{d}{du}\left(w_j^\top \nabla C\right) = 0. \tag{35}$$

Note that

$$\frac{d}{du}\left(\nabla C\right) = \left(\frac{\partial \nabla C}{\partial c}\right)\frac{dc}{du}. \tag{36}$$

The term $\partial\nabla C/\partial c$ is an $M \times L$ matrix with elements $\partial^2 C/\partial K_m \partial c_l$. To simplify notation, we define the matrix Λ with elements

$$\Lambda_{ml} = \frac{\partial^2 C}{\partial K_m \partial c_l}. \tag{37}$$

Therefore, the $R + 1 = M$ equations that must be satisfied as c is varied over u are Eq. (31) and

$$w_j^\top \Lambda \frac{dc}{du} = 0 \qquad \forall j = 1, \ldots, R, \tag{38}$$

where Eq. (38) relies on $dw_j/dc = 0$ which results from $P_{i\to f}$ and $\nabla P_{i\to f}$ being independent of c [c.f., Eq. (9)]. Eqs. (31) and (38) are both of the form $p^\top dc/du = 0$

where p is a length-L vector. An $L \times M$ matrix Ω can be formed from the M equations arising from (31) and (38), where

$$\Omega = \begin{pmatrix} | & & | \\ p_1 & \ldots & p_M \\ | & & | \end{pmatrix}. \tag{39}$$

Then, an $L \times L$ projector (matrix) $\mathcal{P}_\Omega$ is defined as

$$\mathcal{P}_\Omega = \mathbb{1} - \Omega(\Omega^\top \Omega)^{-1}\Omega^\top, \tag{40}$$

where the matrix $\Omega^\top \Omega$ is assumed to be full rank. We have the following differential equation for $c(u)$:

$$\frac{dc}{du} = \mathcal{P}_\Omega h. \tag{41}$$

Upon starting with a local isolated trap, the function h can be chosen in an attempt to either create (i) a trap level set for traversal or (ii) a saddle for further climbing of the landscape. Below, these two goals are addressed by specifying that h extremize the ancillary cost function $\mathcal{L}_1$ or $\mathcal{L}_2$, respectively.

(i) Creation of a level set. For the goal of converting the original constraint-induced isolated trap into a level set (i.e., Fig. 1a → b), we employ the cost function

$$\mathcal{L}_1 = \mathrm{Tr}(\tilde{\mathcal{H}}^2) = \sum_j \left(\tilde{\lambda_j}\right)^2. \tag{42}$$

Minimization of $\mathcal{L}_1$ implies reduction of the projected Hessian eigenvalues $\tilde{\lambda_j}$ towards zero, thereby allowing for creation of a trap level set. In practice, the generation of even one non-trivial zero eigenvalue $\tilde{\lambda_j}$ (i.e., beyond the constraint-induced trivial zero eigenvalue of $\tilde{\mathcal{H}}$ discussed in 2.3) via minimization of $\mathcal{L}_1$ would suffice for opening up a level set (see Fig. 1b). In order to identify h, we differentiate $\mathcal{L}_1$,

$$\frac{d\mathcal{L}_1}{du} = \left(\frac{\partial \mathcal{L}_1}{\partial c}\right)^\top \frac{dc}{du} \tag{43}$$

$$= \left(\frac{\partial \mathcal{L}_1}{\partial c}\right)^\top \mathcal{P}_\Omega h, \tag{44}$$

and set $h = -\partial \mathcal{L}_1 / \partial c$ to minimize $\mathcal{L}_1$.

(ii) Creation of a saddle. For the goal of transforming an isolated trap into a saddle (i.e., Fig. 1a → c), we seek to make the constrained Hessian $\mathcal{H}$ indefinite. The creation of a positive Hessian eigenvalue may permit a control trajectory to 'escape' the original isolated trap by climbing the landscape using the first-order constrained D-MORPH procedure described in Sect. 2.1 after taking a small step away from the critical point along the appropriate saddle-increasing direction. For this objective we utilize the cost function

$$\mathcal{L}_2 = \mathrm{tr}(\mathcal{H}) = \sum_j \lambda_j, \tag{45}$$

where maximizing $\mathcal{L}_2$ over an excursion of $c(u)$ aims to create at least one positive constrained Hessian eigenvalue. Maximization of $\mathcal{L}_2$ is accomplished by setting $h = \partial\mathcal{L}_2/\partial c$, although there is generally no assurance that a positive eigenvalue will develop by morphing $c(u)$. Here we use the constrained (i.e., not the projected) Hessian based on the desire to alter the eigenstructure of $\mathcal{H}$ without any concern towards also creating a level set as in case (i) above.

Section 3 presents examples illustrating the transformations from an isolated trap to a level set (Fig. 1a $\to$ b) as well as to a saddle (Fig. 1a $\to$ c).

3 Numerical illustrations

The simulations below utilize systems of low-dimension N for simple illustration of the concepts presented in Sect. 2. The constraints imposed are motivated by their dynamic counterparts and others could be considered as well. To that end, extensive additional studies will be needed to thoroughly assess the impact of limited resources on achieving optimal control and on constraint-induced landscape topology. In the simulations below, several different constraints are employed to show the diversity of suboptimal critical point landscape topologies, and the constraint parameters c will be specified for each case. Maximization of $P_{1\to N}$ is considered, as the $|1\rangle \to |N\rangle$ transition is most likely a demanding goal when constraints are imposed on the controls. As discussed in Sect. 1, it is possible to transfer from constrained kinematic controls to dynamic controls using Eq. (6) [6]. The present paper will not explore this transfer, but the ability to do so provides an important foundation for the kinematic analysis [7].

3.1 Exploring a trap resulting from an insufficient number of controls

Many resource limited traps were found to be isolated points on the landscape as in Fig. 1a (Sects. 3.2 and 3.3 give two examples). However, some constraints directly produced trap level sets as indicated in Fig. 1b. In order to illustrate this latter circumstance, the first type of constraint considered here is a reduction in the number of admitted control variables to $\tilde{M}$, where $\tilde{M} \leq N(N+1)/2$ [c.f., Eq. (7)]. Figure 2a, b show the monotonic increase in $P_{1\to 6}$ during an optimization and the corresponding evolution of the kinematic control variables, respectively, for an $N = 6$ dimensional system with $\tilde{M} = 2N - 2 = 10$ control variables and the remaining 11 matrix elements of A held fixed at randomly generated initial values. Importantly, the fixed elements included all A_{1j}, $j = 1, \ldots, N = 6$, which places a substantial limitation on the ability to move population out of the initial state $|1\rangle$. These, and the

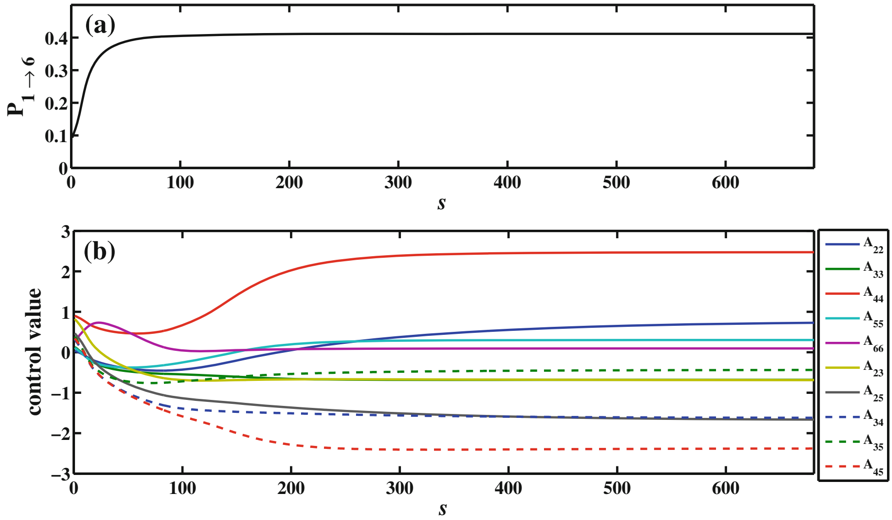

Fig. 2 **a** Monotonic increase in $P_{1\to6}$ for an $N = 6$ dimensional system where $2N - 2 = 10$ control variables are utilized and the remaining elements of A are held fixed at randomly generated initial values. A trap is encountered at $P_{1\to6} = 0.411$. **b** (Color available online) Evolution of the control variables

additional fixed variables (A_{24}, A_{26}, A_{36}, A_{46}, A_{56}), prevented complete control and a trap was encountered at $P_{1\to6} = 0.411$, as suggested in Fig. 2a.

Simply employing a reduced number of control variables does not necessitate use of a formal constraint function C as set out in Sect. 2.1. Thus, the Hessian used to explore the local landscape at the encountered trap is a simplified form of the constrained Hessian from Eq. (19), specifically, $\mathcal{H}_{\tilde{\mathcal{M}}} = \nabla^2 P_{1\to6}$ which is an $\tilde{M} \times \tilde{M}$ matrix. The ten eigenvalues of the Hessian are shown in Fig. 3a. Two eigenvalues are very small, $\lambda_9 \sim 10^{-7}$ and $\lambda_{10} \sim 10^{-9}$ and their corresponding eigenvectors ν_9 and ν_{10} are shown in Fig. 3b. These eigenvalues are sufficiently small to permit their associated eigenvectors to locally specify a trap level set that may be traversed by solving the equation

$$\frac{dK}{dr} = \left[\nu_9(r)\nu_9^\top(r) + \nu_{10}(r)\nu_{10}^\top(r)\right] g(r) \tag{46}$$

where $g(r)$ is a function that may be freely chosen to dictate the level set trajectory. Figure 4 shows that the controls move in a coordinated manner on a level set where g was a length-$\tilde{M}$ vector with randomly generated elements. During the level set traversal, the eigenvalues and eigenvectors vary [note the r-dependence in Eq. (46)]. The controls substantially vary over the level set, particularly the elements A_{33}, A_{55}, A_{23} and A_{35}, which contribute heavily to the eigenvectors in Fig. 3b. The highly coordinated changes in the controls dictated by ν_9 and ν_{10} still maintain $P_{1\to6}$ at the trap value. Other level set trajectories were explored on the trap with different choices for $g(r)$ (not shown), and the overall results indicate that the trap level set covers a broad domain on the landscape.

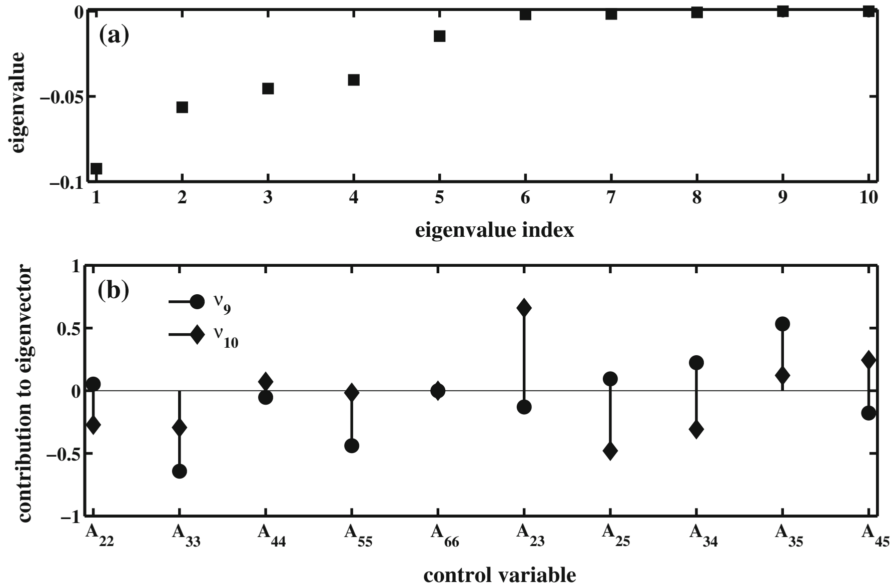

Fig. 3 **a** Hessian eigenvalues at the $P_{1\to6} = 0.411$ trap from Fig. 2. The presence of two nearly zero eigenvalues indicates that the controls may exist on a level set. **b** Eigenvectors ν_9, ν_{10} (shown by their component A_{ij} elements) associated with the two eigenvalues λ_9 and λ_{10} in **a**. Changing the associated control elements in a coordinated fashion indicated by the eigenvectors would constitute movement on the trap level set with $P_{1\to6}$ remaining constant to a specified degree

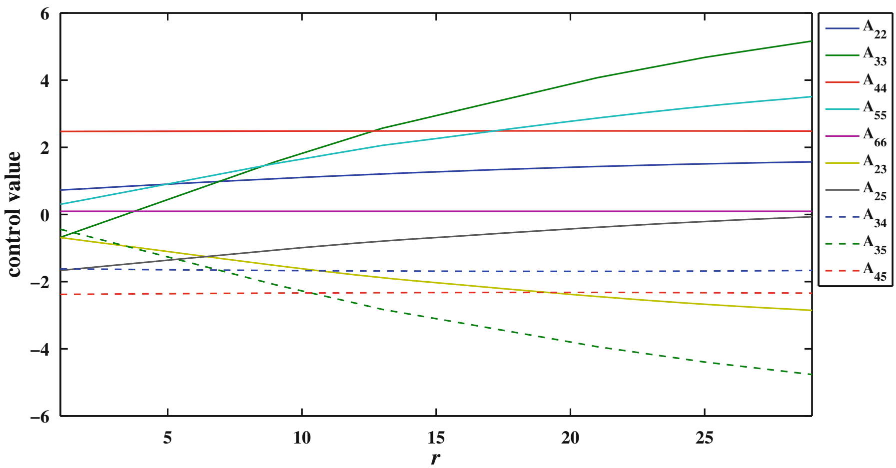

Fig. 4 (Color available online) One of many possible level set trajectories on the trap at $P_{1\to6} = 0.411$ in Figs. 2 and 3. Over the individual variation of the controls on the level set, the $P_{1\to6}$ value is maintained at 0.411 to $\sim 10^{-6}$. The appreciable changes to the controls indicates that the trap lies on a level set of extensive size, implying a degree of robustness to noise

3.2 Local landscape topology at an isolated suboptimal critical point

In the laboratory an important variable is the control fluence F_{dyn},

$$F_{dyn} = \int_{-\infty}^{+\infty} |\varepsilon(\omega)|^2 d\omega, \tag{47}$$

where $\varepsilon(\omega) = \tilde{\varepsilon}(\omega)\exp(\imath\phi(\omega))$ is the Fourier transform of $\varepsilon(t)$ with $\tilde{\varepsilon}(\omega) \geq 0$ being the amplitude and $\phi(\omega)$ the phase. In many settings, the fluence is fixed while seeking an optimal field, however assessing the potential control outcome benefits of varying the fluence is an important issue. A kinematic analog of fluence is denoted by C_F,

$$C_F = \|A\|^2 = \mathrm{Tr}(A^\dagger A). \tag{48}$$

We explore the evolving topology of suboptimal traps as fluence is incrementally increased to enhance the control freedom, thereby resulting in successively higher yields for $P_{i\to f}$. Separate optimizations were performed (c.f., Sect. 2.1) for $N = 4$ dimensional systems at each of the fluence values $C_F = C_0 = 0.1, 2$, and 4, resulting in arrival at suboptimal traps with $P_{1\to 4} = 0.049, 0.708$, and 0.976, respectively. The topology of the respective traps can be assessed by examining the eigenvalues of the constrained Hessian in Eq. (19), which are shown in Fig. 5. In these cases, the constrained Hessian eigenvalues are all negative, showing that each trap is an isolated point on the landscape (i.e., the topology indicated in Fig. 1a). The constrained Hessian eigenvalues show a general shift towards becoming less negative as the fluence increases, and the trace of the constrained Hessian (i.e., the sum of the eigenvalues) increases over the values $-13.82, -10.39, -7.06$ for $C_F = 0.1, 2, 4$, respectively. Thus, the trap at $P_{1\to 4} = 0.049$ is a 'sharper' point than that at $P_{1\to 4} = 0.708$ or 0.976. For these traps, the gradient vector $\nabla P_{1\to 4}$ is approximately zero except for the element $\partial P_{1\to 4}/\partial A_{14}$, which becomes smaller as the landscape is ascended further upon relaxing (increasing) C_F. The constrained Hessian spectrum in Fig. 5 is approaching the expected behavior [22] of the unconstrained Hessian $\nabla^2 P_{1\to 4}$ upon increasing C_F, where $\mathcal{H} \to \nabla^2 P_{1\to 4}$ as $\nabla P_{1\to 4} \to 0$ in Eq. (19). The Hessian with no constraints on the controls has at most $2N - 2 = 6$ non-zero negative eigenvalues at $P_{1\to 4} = 1$, and this behavior is becoming apparent in Fig. 5 as $P_{1\to 4}$ increases.

3.3 Varying suboptimal critical point topology

We now introduce a new constraint,

$$C = \|A - B\|^2 = \mathrm{Tr}\left((A - B)^\dagger (A - B)\right). \tag{49}$$

Keeping C fixed at a specified initial value C_D can be interpreted as A maintaining a fixed distance from a reference set of controls (matrix) B. For an $N = 4$ dimensional system, the following randomly chosen B matrix was employed:

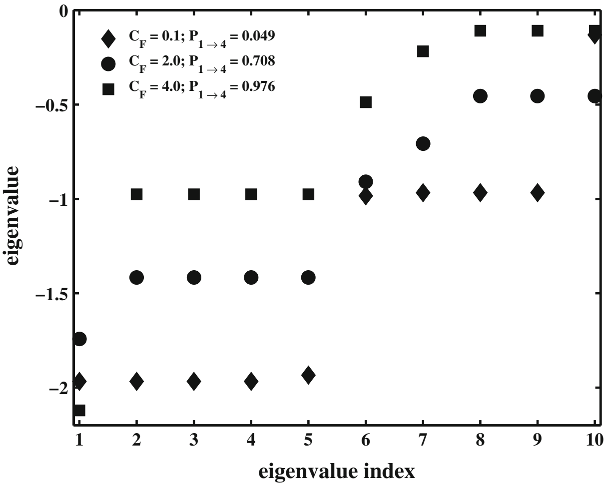

Fig. 5 Constrained Hessian eigenvalues at $P_{1\to4}$ traps resulting from optimization of an $N = 4$ dimensional system with the imposition of a fixed fluence constraint C_F [c.f., Eq. (48)] whose values are shown in the Figure along with the resultant suboptimal $P_{1\to4}$ values. All of the Hessian eigenvalues are negative, such that any change to the control variables would decrease $P_{1\to4}$, indicating that each critical point is isolated with no accompanying level set. As the fluence, and the resultant $P_{1\to4}$ value, increase, the eigenvalue behavior suggests that the theoretically predicted $2N - 2 = 6$ non-zero negative eigenvalues will be present upon reaching the top of the landscape [22]

$$B = \begin{pmatrix} 1.4595 & 1.3964 & 1.3912 & 1.0532 \\ 1.3964 & 1.9300 & 0.8963 & 1.2742 \\ 1.3912 & 0.8963 & 1.0827 & 0.9294 \\ 1.0532 & 1.2742 & 0.9294 & 1.4529 \end{pmatrix}. \tag{50}$$

A randomly generated initial A matrix yielded $C_D = 1.868$; this value for C_D was maintained during a constrained landscape ascent performed using the technique from Sect. 2.1 along with B in Eq. (50). Figure 6a shows the landscape ascent with A acting as the control and (b) shows the evolution of the controls up until a trap is encountered at $P_{1\to4} = 0.873$ with the following form for A:

$$A_{trap} = \begin{pmatrix} 1.7252 & 1.5774 & 1.4261 & 0.3417 \\ 1.5774 & 1.5055 & 0.6441 & 1.5277 \\ 1.4261 & 0.6441 & 0.9554 & 1.2323 \\ 0.3417 & 1.5277 & 1.2323 & 1.7389 \end{pmatrix}. \tag{51}$$

The eigenvalues of the corresponding constrained Hessian $\mathcal{H}$ and projected Hessian $\tilde{\mathcal{H}}$ [c.f., Eqs. (19) and (23), respectively] are shown in Fig. 7a, b, respectively. All constrained Hessian $\mathcal{H}$ eigenvalues are negative, and only one zero projected Hessian $\tilde{\mathcal{H}}$ eigenvalue is present, which corresponds to the 'trivial' zero eigenvalue introduced by the projector $\mathcal{P}_{\nabla C}$ [c.f., Eq. (23)]. Thus, this trap has the topology suggested in Fig. 1a and does not form a level set, and any variation to the controls will result in a decrease in $P_{1\to4}$. The following Subsections will utilize the methods presented in

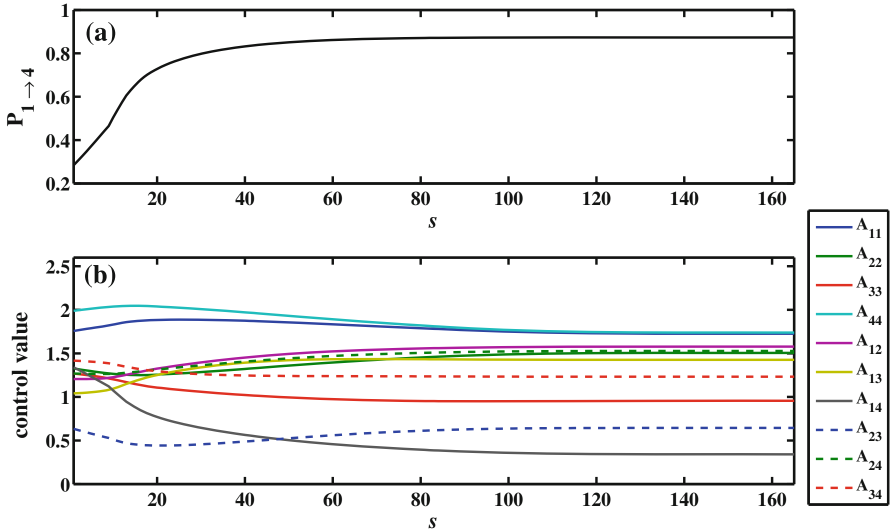

Fig. 6 **a** Increase in $P_{1\to4}$ when $C_D = 1.868$ is fixed along with B in Eq. (50). A trap is encountered at $P_{1\to4} = 0.873$. **b** (Color available online) Evolution of control variables during initial landscape ascent. Upon maximizing $P_{1\to4}$, the control variable A_{14} changes most significantly

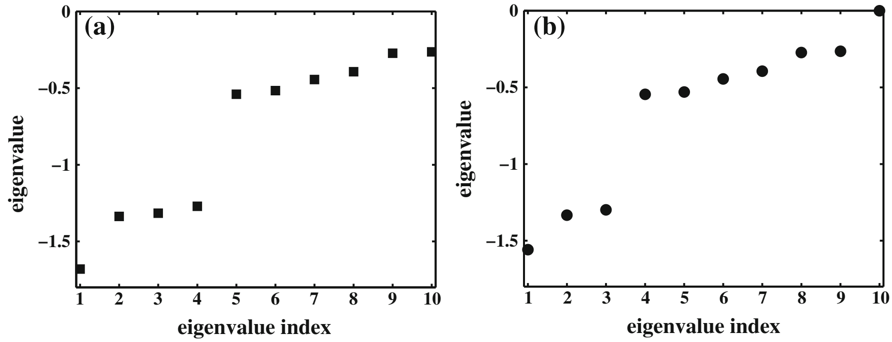

Fig. 7 **a** Eigenvalues of the constrained Hessian at the trap identified in Fig. 6. All eigenvalues are negative, indicating that the trap is an isolated point. **b** Eigenvalues of the projected constrained Hessian. The one identically zero eigenvalue results from the introduction of the projector $\mathcal{P}_{\nabla C}$ [c.f., Eq. (23)] with a single imposed constraint

Sect. 2.4 to vary the *form* of the constraint to convert this isolated trap into either (i) a level set or (ii) a saddle.

3.3.1 Transforming an isolated trap into a level set: changing Fig. 1a into Fig. 1b

The trap encountered at $P_{1\to4} = 0.873$ with the forms of A_{trap} and B in Eqs. (51) and (50), respectively, was identified to be an isolated point on the control landscape, as indicated by the negative constrained Hessian eigenvalues shown in Fig. 7a. By considering B as comprising the constraint parameters, that is, $c = [B_{11}, B_{12}, \ldots, B_{44}]$ (c.f., Sect. 2.1), the morphing procedure from Sect. 2.4 was employed to determine whether

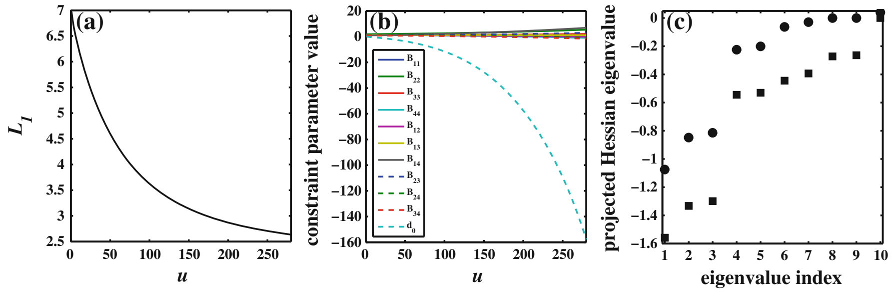

Fig. 8 Starting from the trap in Fig. 6, plot **a** shows the decrease in $\mathcal{L}_1$ [c.f., Eq. (42)] as the constraint parameters B and d_0 are morphed, as shown in plot (**b**), in an effort to identify a projected Hessian $\tilde{\mathcal{H}}$ null space. **c** Corresponding changes in projected Hessian $\tilde{\mathcal{H}}$ eigenvalues, evolving from squares to circles over the range of u in (**a**) and (**b**). Color for (**b**) available online

a trap level set could be created by varying B. However, in doing so with $C = C_D$ fixed, no discernible change was observed in the trap topology. An additional variable d_0 was introduced such that $c = [B_{11}, B_{12}, \ldots, B_{44}, d_0]$, where

$$C_D = \|A - B\|^2 + d_0 = \mathrm{Tr}\left((A - B)^\dagger (A - B)\right) + d_0 \tag{52}$$

with $d_0 = 0$ in the initial first-order D-MORPH landscape ascent (i.e., to reach the original trap in Fig. 6); this procedure is equivalent to morphing $C_D - d_0(u)$ as the extra constraint variable (while C_D is held fixed). This new set c of constraint parameters was then used to minimize $\mathcal{L}_1$ from Eq. (42) while keeping $C_D = 1.868$ fixed at its original value. Employing the prescription in Sect. 2.4, we have the following: c is parametrized by the variable u, A is held fixed [at Eq. (51)], $P_{1\to 4}$ and C_D are maintained at 0.873 and 1.868, respectively, and the gradients $\nabla P_{i\to f}$ and ∇C_D are forced to remain parallel by the structure of dc/du [c.f., Eq. (41)]. Figure 8a shows the monotonic decrease in $\mathcal{L}_1$ as B and d_0 vary in Fig. 8b. $\mathcal{L}_1$ decreases from 6.97 to 2.64, while $C_D = 1.868$ was maintained on the order of 10^{-5}. The final resultant B matrix was

$$B_{level\ set} = \begin{pmatrix} -0.7317 & -0.0952 & 1.1039 & 6.9185 \\ -0.0952 & 5.4296 & 2.9756 & -0.8164 \\ 1.1039 & 2.9756 & 2.1324 & -1.5684 \\ 6.9185 & -0.8164 & -1.5684 & -0.9053 \end{pmatrix}, \tag{53}$$

and d_0 changed from 0 to -157.8. Figure 8c shows the shift in projected Hessian $\tilde{\mathcal{H}}$ eigenvalues during the constraint parameter morphing, and the simulation was terminated at the appearance of a non-trivial zero eigenvalue on the order of 10^{-4}. The projected Hessian eigenvalues overall shift to be less negative as the constraint parameters vary. As shown in Fig. 8c, a slightly positive $\tilde{\mathcal{H}}$ eigenvalue also appears, which is not strictly prohibited during the minimization of $\mathcal{L}_1$. Its magnitude is approximately the same as the smallest negative eigenvalue.

The new constraint parameters identified above were then used to begin a level set traversal, where the goal was to vary elements of A starting from Eq. (51) on the newly created trap level set while $B = B_{level\ set}$, $d_0 = -157.8$, and $C_D = 1.868$ were fixed. The level set traversal was terminated when $P_{1\to4}$ deviated from 0.873 on the order of 10^{-4}. The elements of A changed by a few percent (e.g., A_{14} varied from 0.342 to 0.311, a change of ∼9 %) and all elements differ from their values in Eq. (51), indicating that there is a connected family of controls that reside on a level set to the specified precision. In this particular example, the free function g' in Eq. (29) was randomly generated, and simulations using other free functions provided additional A matrices that were on the level set (not shown).

3.3.2 Transforming an isolated trap into a saddle: changing Fig. 1a into Fig. 1c

As a final implementation of the techniques from Sect. 2.4, the isolated trap [with A from Eq. (51)] was converted to a saddle, where the constraint parameters $c = [B_{11}, \ldots, B_{44}, d_0]$ were varied as a function of u so as to maximize $\mathcal{L}_2$ in Eq. (45) starting from Eq. (50) and $d_0 = 0$. Figure 9a shows the evolution of these constraint parameters where $\mathcal{L}_2$ increased from −8.03 to −3.88; consequently, the constrained Hessian eigenvalues, shown in Fig. 9b, increased (changing from squares to circles). The inset in (b) shows the appearance of two distinctly positive constrained Hessian eigenvalues. Here, $C_D = 1.868$ was maintained on the order of 10^{-4}, and B evolved to

$$B_{saddle} = \begin{pmatrix} -3.9120 & -2.2603 & 0.6869 & 15.4317 \\ -2.2603 & 10.5090 & 5.9936 & -3.8506 \\ 0.6869 & 5.9936 & 3.6559 & -5.1936 \\ 15.4317 & -3.8506 & -5.1936 & -4.3279 \end{pmatrix} \tag{54}$$

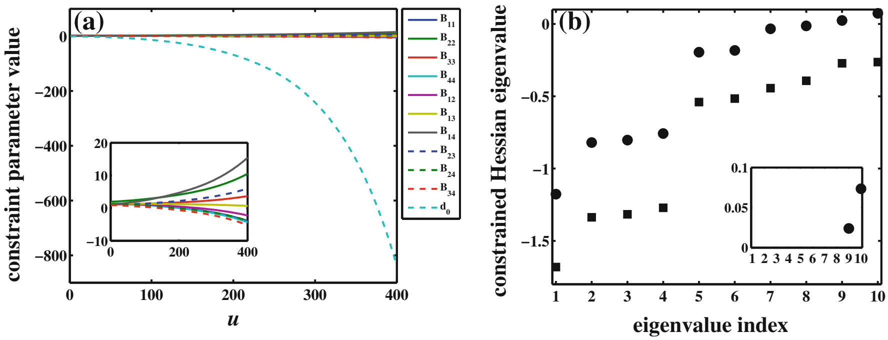

Fig. 9 Starting from the trap in Fig. 6, plot **a** shows the changes in constraint parameters B and d_0 as $\mathcal{L}_2$ [c.f., Eq. (45)] increases in an effort to identify at least one positive constrained Hessian eigenvalue. The constrained Hessian eigenvalues evolve in (**b**), changing from squares to circles over the range of u in (**a**). The *inset* in (**b**) shows that two eigenvalues have become significantly positive. Color for (**a**) available online

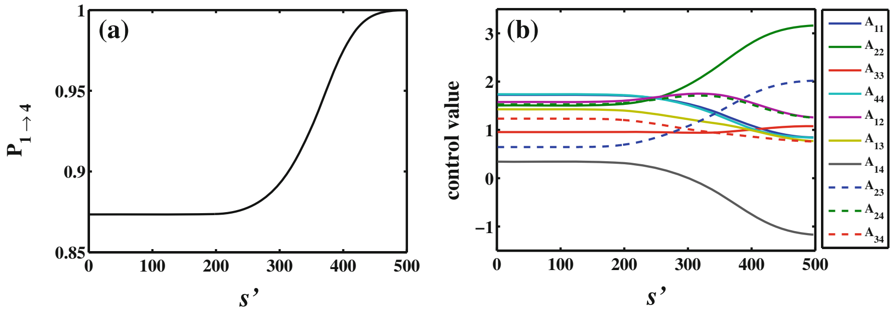

Fig. 10 **a** Increase in $P_{1\rightarrow4}$ after identification of positive constrained Hessian eigenvalues in Fig. 9. The $P_{1\rightarrow4}$ trajectory is obtained using the first-order constrained D-MORPH technique presented in Sect. 2.4. **b** (Color available online) Evolution of the control variables

with d_0 dramatically changing from 0 to -838.7 to compensate for the change in B and $\|A - B\|^2$ ($\|B_{saddle}\|^2 \sim 801$). At the end of the constraint morphing procedure, the first-order constrained D-MORPH method was again employed (now over the variable s') to see if $P_{1\rightarrow4}$ would increase upon implementation with the newly created B_{saddle} and $d_0 = -838.7$. Figure 10 shows the eventual full ascent of the $P_{1\rightarrow4}$ landscape (10a) as the controls A evolve (10b) from Eq. (51). Nominally a step along a positive Hessian eigenvector would be required to initiate the climb away from the saddle, but the first-order D-MORPH algorithm was able to still climb from a slow start as depicted in Fig. 10a.

4 Conclusions

This work developed methodologies to explore the neighborhood around suboptimal resource limited traps on the quantum control landscape. Through numerical simulations using kinematic controls and a state-to-state transition probability observable, it was shown that some traps exist as isolated points on the landscape while others lie on a submanifold of suboptimal solutions. The latter case can be viewed as representing suboptimal constrained controls exhibiting some degree of robustness, which has important laboratory implications. This work presented a means to change the local landscape topology at suboptimal critical points by systematically relaxing the constraints to address the trade-off between limited resources and landscape behavior. The relaxation process permitted (i) searching for level sets of observable-preserving controls through the identification of (at least one) direction of zero landscape curvature, and (ii) seeking a saddle feature by the identification of a direction of positive curvature, which could then be exploited to further ascend the landscape to achieve an improved yield.

This work utilized kinematic controls as a means to simplify the analysis and manipulation of the constrained control landscape. As discussed in Sect. 1, a set of constrained kinematic controls constituting a suboptimal trap can be mapped to a set of dynamic controls through, for example, a target unitary transformation [c.f., Eq. (6)]. However, it is important to note that the mapping metric represented by Eq. (6) does not necessarily guarantee that the mapped dynamic controls maintain trap-specific topological features such as a negative definite Hessian spectrum. Conserving higher-order topological properties through a kinematic → dynamic mapping procedure is a complex and demanding task, and as an alternative one may directly apply the constrained control procedures from this work to dynamic controls with the understanding that this latter goal can be computationally costly due to the typical high-dimensionality of the dynamic control variable landscape. The mapping procedure and direct application of constraints to dynamic controls will be explored in forthcoming work [7], where both routes offer the prospect of opening up new avenues for investigating the diversity of constrained dynamic controls and ultimately their implications in the laboratory.

Acknowledgments A.D. acknowledges support from the Program in Plasma Science and Technology at Princeton University and thanks David Hocker (Princeton University) for his assistance in generating Fig. 1. The authors thank Professor Carey Rosenthal (Drexel University) for insightful discussions. We also acknowledge support from the DOE (Grant Number DE-FG-02-02ER15344), NSF (Grant Number CHE-1058644), and the ARO (Grant Number W911NF-13-1-0237).

References

1. M. Abe, Y. Ohsuki, Y. Fujimura, Z. Lan, W. Domcke, Geometric phase effects in the coherent control of the branching ratio of photodissociation products of phenol. J. Chem. Phys. **124**, 224316 (2006)
2. C. Brif, R. Chakrabarti, H. Rabitz, Control of quantum phenomena: past, present and future. New J. Phys. **12**, 075008 (2010)
3. G. Cerullo, S. Silvestri, Ultrafast optical parametric amplifiers. Rev. Sci. Instrum. **74**, 1 (2003)
4. P. Domachuk, N.A. Wolchover, M. Cronin-Golomb, A. Wang, A.K. George,C.M.B. Cordeiro, J.C. Knight, F.G. Omenetto, Over 4000 nm bandwidthof mid-ir supercontinuum generation in sub-centimeter segments ofhighly nonlinear tellurite pcfs. Opt. Express *16*, 7161 (2008).doi:10.1364/OE.16.007161. http://www.opticsexpress.org/abstract.cfm?URI=oe-16-10-7161
5. D. Dong, I. Petersen, Quantum control theory and applications: a survey. IET Control Theory Appl. **4**, 2651 (2010)
6. A. Donovan, V. Beltrani, H. Rabitz, Exploring the impact of constraints in quantum optimal control through a kinematic formulation. Chem. Phys. **425**, 46 (2013)
7. A. Donovan, H. Rabitz, Exploring constrained dynamic control variables in quantum control (2013, in preparation)
8. J. Dudley, G. Genty, S. Coen, Supercontinuum generation in photonic crystal fiber. Rev. Mod. Phys. **78**, 1135 (2006)
9. K.D. Greve, P. McMahon, D. Press, T. Ladd, D. Bisping, C. Schneider, M. Kamp, L. Worschech, S. Höfling, A. Forchel, Y. Yamamoto, Ultrafast coherent control and suppressed nuclear feedback of a single quantum dot hole qubit. Nat. Phys. **7**, 872 (2011)
10. F. Grossman, L. Feng, G. Schmidt, T. Kunert, R. Schmidt, Optimal control of a molecular cis-trans isomerization model. Europhys. Lett. **60**, 201 (2002)
11. R. Hildner, D. Brinks, N. van Hulst, Femtosecond coherence and quantum control of single molecules at room temperature. Nat. Phys. **7**, 172 (2010)
12. M. Lapert, R. Tehini, G. Turinici, D. Sugny, Monotonically convergent optimal control theory of quantum systems with spectral constraints on the control field. Phys. Rev. A **79**, 063411 (2009)
13. J. Möhring, T. Buckup, M. Motzkus, A quantum control spectroscopy approach by direct UV femtosecond pulse shaping. IEEE J. Sel. Top. Quantum Electron. **18**, 449 (2012)
14. K. Moore, H. Rabitz, Exploring constrained quantum control landscapes. J. Chem. Phys. **137**, 134113 (2012)
15. K. Moore, M. Hsieh, H. Rabitz, On the relationship between quantum control landscape structure and optimization complexity. J. Chem. Phys. **128**, 154117 (2008)
16. K. Moore, H. Rabitz, Exploring quantum control landscapes: topology, features, and optimization scaling. Phys. Rev. A **84**, 012109 (2011)

17. K. Moore, C. Brif, M. Grace, A. Donovan, D. Hocker, T.S. Ho, R. Wu, H. Rabitz, Exploring the tradeoff between fidelity and time optimal control of quantum unitary transformations. Phys. Rev. A **86**, 062309 (2012)
18. A. Natan, U. Lev, V. Prabhudesai, B. Bruner, D. Strasser, D. Schwalm, I. Ben-Itzhak, O. Heber, D. Zajfman, Y. Silberberg, Quantum control of photodissociation by manipulation of bond softening. Phys. Rev. A **86**, 043418 (2012)
19. A. Peirce, M. Dahleh, H. Rabitz, Optimal control of quantum-mechanical systems: existence, numerical approximation, and applications. Phys. Rev. A **37**, 4950 (1988)
20. H. Rabitz, M. Hsieh, C. Rosenthal, Quantum optimally controlled transition landscapes. Science **303**, 1998 (2004)
21. H. Rabitz, M. Hsieh, C. Rosenthal, Landscape for optimal control of quantum-mechanical unitary transformations. Phys. Rev. A **72**, 052337 (2005)
22. H. Rabitz, T.S. Ho, M. Hsieh, R. Kosut, M. Demiralp, Topology of optimally controlled quantum mechanical transition probability landscapes. Phys. Rev. A **74**, 012721 (2006)
23. V. Ramakrishna, M. Salapaka, M. Dahleh, H. Rabitz, A. Pierce, Controllability of molecular systems. Phys. Rev. A **51**, 960 (1995)
24. J. Roslund, H. Rabitz, Gradient algorithm applied to laboratory quantum control. Phys. Rev. A **79**, 053417 (2009)
25. A. Rothman, T.S. Ho, H. Rabitz, Observable-preserving control of quantum dynamics over a family of related systems. Phys. Rev. A **72**, 023416 (2005)
26. A. Rothman, T.S. Ho, H. Rabitz, Exploring the level sets of quantum control landscapes. Phys. Rev. A **73**, 053401 (2006)
27. S. Schirmer, H. Fu, A. Solomon, Complete controllability of quantum systems. Phys. Rev. A **63**, 063410 (2001)
28. C.C. Shu, N. Henriksen, Phase-only shaped laser pulses in optimal control theory: application to indirect photofragmentation dynamics in the weak-field limit. J. Chem. Phys. **136**, 044303 (2012)
29. I. Sola, V. Malinovsky, D. Tannor, Optimal pulse sequences for population transfer in multilevel systems. Phys. Rev. A **60**, 3081 (1999)
30. P. von den Hoff, S. Thallmair, M. Kowalewski, R. Siemering, R. de Vivie-Riedle, Optimal control theory-closing the gap between theory and experiment. Phys. Chem. Chem. Phys. **14**, 14460 (2012)
31. J. Werschnik, E. Gross, Tailoring laser pulses with spectral and fluence constraints using optimal control theory. J. Opt. B **7**, S300 (2005)
32. J. Werschnik, E.K.U. Gross, Quantum optimal control theory. J. Phys. B **40**, R175 (2007)
33. S. Zou, G. Balint-Kuri, F. Manby, Vibrationally selective optimal control of alignment and orientation using infrared laser pulses: Application to carbon monoxide. J. Chem. Phys. **127**, 044107 (2007)